Theoretical and experimental investigation of the novel high-pressure form of elemental boron.

Artem R. Oganov[1,2*], Jiuhua Chen[3,4], Carlo Gatti[5], Yanzhang Ma[6], Yanming Ma[1,7], Colin W. Glass[1], Zhenxian Liu[8], Tony Yu[3], Oleksandr O. Kurakevych[9], Vladimir L. Solozhenko[9]

[1] *Laboratory of Crystallography, Department of Materials, ETH Zurich, Wolfgang-Pauli-Str. 10, CH-8093 Zurich, Switzerland.*
[2] *Geology Department, Moscow State University, 119992 Moscow, Russia.*
[3] *Center for the Study of Matters at Extreme Conditions and Department of Mechanical and Materials Engineering, Florida International University, Miami, FL 33199, USA*
[4] *Mineral Physics Institute and Department of Geosciences, Stony Brook University, Stony Brook, NY 11794-2100, USA*
[5] *CNR-ISTM Istituto di Scienze e Tecnologie Molecolari, via Golgi 19, 20133 Milano, Italy.*
[6] *Department of Mechanical Engineering, Texas University of Technology, 7th St. & Boston Ave., Lubbock, Texas 79409, USA.*
[7] *National Lab of Superhard Materials, Jilin University, Changchun 130012, P. R. China.*
[8] *Geophysical Laboratory, Carnegie Institution of Washington, Washington, DC 20015, USA*
[9] *LPMTM-CNRS, Université Paris Nord, Villetaneuse, F-93430, France*

**Now at: Department of Geosciences and New York Center for Computational Science, Stony Brook University, Stony Brook, NY 11794-2100, USA.*

$1. Details of evolutionary simulations. Evolutionary algorithms are well-suited for the task of crystal structure prediction: using "learning" from the history of the simulation, evolution guides search towards low-energy structures; improving the results from generation to generation, such simulations "zoom" in on the most promising part of the energy landscape until the lowest-energy structure is found. All evolutionary simulations were performed with the USPEX method[30,4,5], using VASP for structure relaxation and energy calculations. As a test, we first ran a variable-cell run with 12 atoms/cell at 1 atm, which correctly produced the α-B_{12} structure as most stable for this system size.

The first generation of structures (population size: 10-50 structures, increasing with system size) was always produced randomly. All produced structures were relaxed; the appropriate thermodynamic potential (total energy at constant volume and 0 K, enthalpy at constant pressure and 0 K) was used as fitness function. Every subsequent generation was produced from the best 60% of the previous generation. New structures were created by heredity (i.e. combining spatially coherent slabs cut from two parent structures in a random direction at random positions and with random thicknesses) and, for variable-cell simulations, 15% of the new structures were obtained using lattice mutation (with Gaussian strength 0.5-0.7, see Ref. 4,5). In addition, the best structure of each generation was carried over into the next generation. Numerous tests show[4] that for systems with ~20 atoms/cell the global minimum (which, for well-known test cases, is the experimentally known stable structure) is usually reached well within ~20 generations (~600 local optimizations).

To solve the structure of γ-B_{28}, we searched for the global energy minimum under constraint of experimental cell parameters. From densities of other boron phases, we estimated the number of atoms in the cell to be between 24 and 32. Since this number has to be even to produce an insulating state, we considered cases of 24, 26, 28, 30 and 32 atoms/cell. Each generation consisted of 50 structures, simulations were run for over 30 generations (but the optimal structures were always found within 11 generations). The 28-atom *Pnnm* structure (Fig. S1) had the lowest energy per atom, correct orthorhombic symmetry, and relaxed cell parameters and diffraction pattern in good agreement with experiment.

Variable-cell evolutionary simulations were performed at 100 GPa and 300 GPa, with 2, 3, 4, 6, 8, 9, 12, 16 atoms/cell and searched for the minimum-enthalpy structure. The population size was between 10 structures (for 2 atoms/cell) and 48 structures (for 16 atoms/cell). These calculations unambiguously indicated the α-Ga-type structure (Fig. S2) as stable.

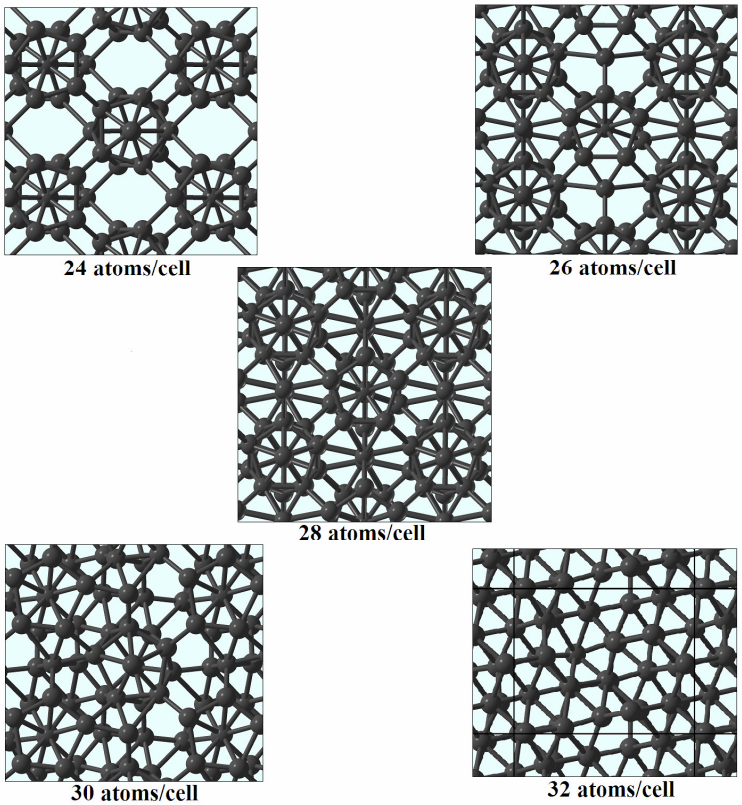

Fig. S1. Best structures obtained with 24, 26, 28, 30, 32 atoms/cell. At experimental cell parameters, the lowest-energy structure contains 28 atoms/cell. The other structures are higher by 0.21 eV/atom (for 24 atoms/cell), 0.10 eV/atom (26 atoms/cell), 0.16 eV/atom (30 atoms/cell), 0.22 eV/atom (32 atoms/cell).

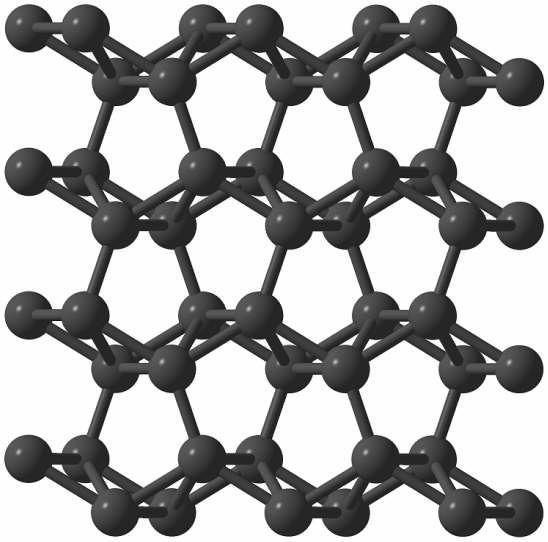

Fig. S2. α-Ga-type structure found in evolutionary simulations at 100 GPa and 300 GPa.

$2. Illustration of an evolutionary simulation: Making icosahedra by evolution. Fig. S3 shows the sequence of best structures in each generation for the 24-atom system at fixed experimental cell parameters. The first (random) generation did not contain any icosahedral structures. Increasingly large fragments of the icosahedra appear in generations 2 and 3, and at the 11th generation the lowest-energy structure is found. This structure becomes identical to α-B_{12} after full relaxation.

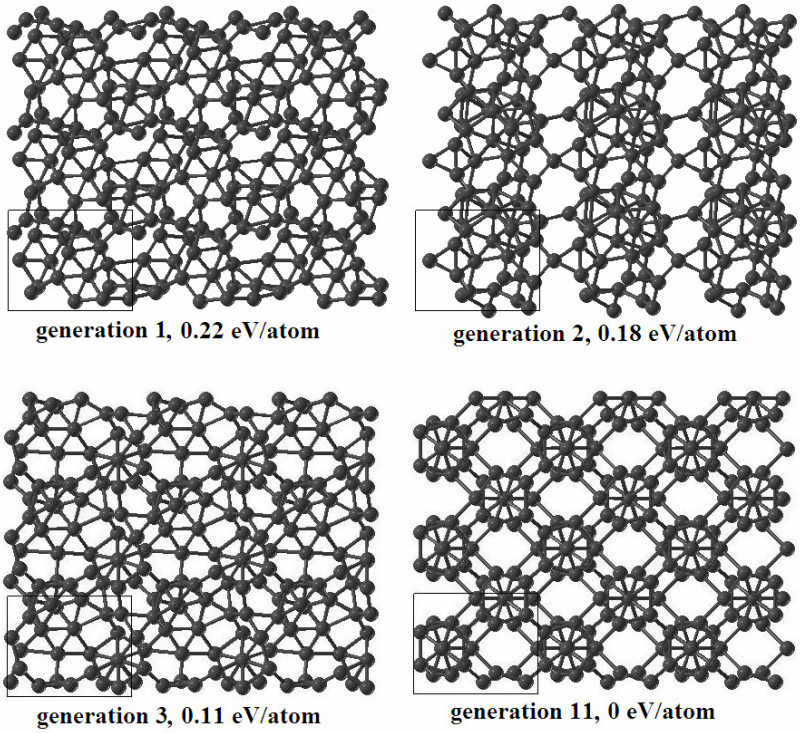

Fig. S3. Example of an evolutionary simulation (24-atom system at fixed cell parameters). Best structure at each generation is shown (with total energies relative to the final energy). Black rectangle shows the unit cell dimensions.

$3. Lattice dynamics calculations and dynamical stability of the γ-B_{28} structure. Using density-functional perturbation theory[25], as implemented in the ABINIT code[26], we have calculated phonon dispersion curves and phonon density of states of the γ-B_{28} phase. Interatomic force constants were determined on a 2x2x2 q-grid (corresponding to a 224-atom supercell) and, in combination with the calculated Born effective charge tensors and dielectric constants, were used to calculate phonon frequencies throughout the Brillouin zone. The resulting phonon

dispersion curves and the phonon density of states are shown in Fig. S4. There are no soft modes and the structure is dynamically stable. Similar lattice dynamics calculations were performed also for α-B_{12} and α-Ga-type phases of boron, and demonstrated that they have no soft modes within their stability fields shown in Fig. 3.

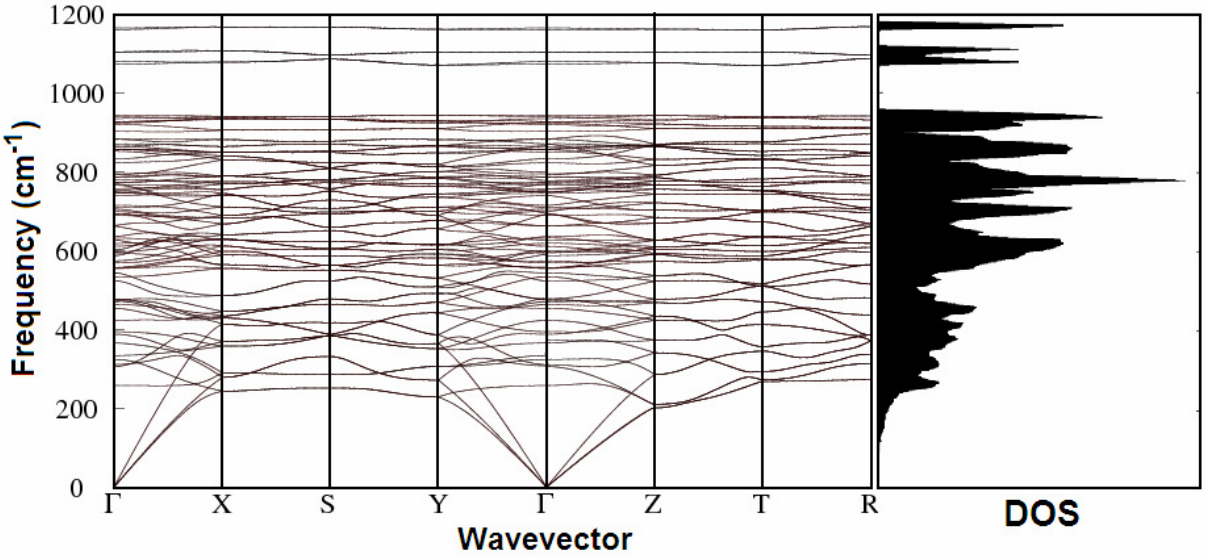

Fig. S4. Phonon dispersion curves and density of states in the γ-B_{28} structure. The phonon density of states contains two sets of very narrow bands, separated from the other bands by pronounced gaps.

$4. Bader analysis (Ref.16).

Robustness of Bader charges. Bader charges are determined solely by the ED distribution, rather than by arbitrary partitioning of the wavefuction contributions. For this reason, their sensitivity to the basis set is not very large. For example, with a triple-ζ basis set the charge of the $(B1)_2$ pair is +0.358, whereas with the quadruple-ζ basis used here it is equal to +0.341, and with another (more complete and flexible) quadruple-ζ basis, derived from the aug-ccpvQZ basis, it is equal to +0.384. The value obtained using the PAW method (+0.484) is likely to be the most accurate one, close to the basis set limit.

The negative charge on the B2 atoms is somewhat more sensitive: its values are -0.300 with the triple-ζ basis set, -0.143 with the quadruple-ζ basis set used here, and -0.152 with the quadruple-ζ basis derived from the aug-ccpvQZ basis. The value obtained using the PAW method (-0.168) is, within uncertainties, equal to the quadruple-ζ basis values.

Bader charges are rather insensitive to the details of the exchange-correlation functional. Using the quadruple-ζ basis set and the LDA exchange-correlation functional[31], we get very similar Bader charges: e.g. +0.338 for the $(B1)_2$ pair, -0.142 for the B2 atoms.

Technical details of Bader analysis. LCAO calculations are the main tool for Bader analysis (integration of atomic volumes and charges and investigation of bond critical points) reported here. All-electron LCAO densities were analysed using the TOPOND code[32,33], which is interfaced to CRYSTAL. Integrated charges and volumes with TOPOND are very accurate, within 0.01 and 0.1 a.u., for charges and volumes, respectively, and with a magnitude of the integrated Laplacian never exceeding 0.004 a.u. Location of critical points and evaluation of their properties is performed using fully analytical density derivatives and density interpolation techniques are not needed. The gradient of the density at critical point locations never exceeds 10^{-15} a.u.

We used uniform grids (200x224x280 for γ-B_{28}, 200x200x200 for α-B_{12}) with PAW densities and atom-centred grids with LCAO densities (308 angular and 120 radial points for the innermost part of the atomic basin, with a fixed radius of 0.59 Å; 1536 angular and a variable number of radial points for the outermost part, with each radial length, associated with a given angular point, determined by the zero-flux surface condition). In the case of PAW densities, charge symmetrisation and density interpolation techniques enabled us to obtain precise (within 0.01 |e|) Bader charges. PAW densities were obtained as a sum of core and valence densities and were analysed using the code presented in Ref. 34. We have verified that the two methods are consistent – i.e. for the same ED distribution the code of Ref. 34 and TOPOND produce identical Bader charges. For instance, for the LCAO density obtained with the quadruple-ζ basis set the two methods give +0.338 and +0.341, respectively, and for the charge of the B2 atom the values are -0.147 and -0.143, respectively.

Tables S1-S3 report some of our results obtained with LCAO calculations. Table S1 shows the properties of the density at (3,-1) bond critical points. One can notice a large difference between the ellipticities of 2-centre and 3-centre bonds – nearly zero ellipticity in the former, and large (>2) ellipticity in the latter case. Interestingly, the most electronegative atoms (B2) form the largest number of elliptic 3-centre bonds (seven), whereas the most electropositive atoms (B1) have only two such bonds. The Laplacian of the density at the bond critical point ($\nabla^2\rho_{bcp}$) is strongly negative (-0.38-0.29 a.u.) for short 2-centre bonds, moderately negative for 3-centre

bonds (-0.13-0.11 a.u.), and very slightly negative (-0.05 a.u.) for the B1-B2 bonds (as expected for polar covalent bonds)

Tables S2 and S3 show the large asymmetry of the bond critical points in the full self-consistent density (Table S2) and a much smaller asymmetry in the IAM model (Table S3). We examined the bond asymmetry parameter:

$$a = 1 - \frac{r_{bcp-B2}}{r_{bcp-B1}},$$

where r_{bcp-B1} and r_{bcp-B2} are distances from the bond critical point to atoms B1 and B2, respectively. For normal intra- and intericosahedral bonds a=0-4%; for the "ionic" B1-B2 bond it reaches 20% (in the IAM model it is only 0% and 4%, respectively).

In γ-B_{28}, atomic charges are correlated with coordination numbers, which, according to Bader analysis are lowest (four) for the positively charged B1 atoms and highest (seven) for the negatively charged B2 atoms (nearly-neutral B3-B5 atoms are six-coordinate). Such correlation between the ionisation state, ionic radius and coordination number is well known for ionic and polar covalent crystals. Autoionization helps to adjust the ionic sizes for optimally dense packing and provides extra stabilisation energy (*ca* -0.06 eV/atom for charges from Table 1).

Table S1. Summary of bond properties in γ-B_{28}. All quantities are in a.u., except bond lengths, n represents the number of bonds of a given type formed by each of the B-atom type. $(R_e)_{av}$, $(\rho_b)_{av}$, $(\nabla^2\rho_b)_{av}$, $(\varepsilon_b)_{av}$ are the averages of equilibrium distances, electron densities, Laplacians and ellipticities at the (3,-1) bond critical point, respectively.

B atom type	Type of bonding	n	$(R_e)_{av}$	$(\rho_b)_{av}$	$(\nabla^2\rho_b)_{av}$	$(\varepsilon_b)_{av}$
B1	within $(B1)_2$ units	1	1.732	0.139	-0.288	0.021
	B1-B2 (3MR)	2	1.903	0.085	-0.052	2.271
	B1-B4	1	1.674	0.156	-0.365	0.038
B2	intra-icosahedral	5	1.798	0.115	-0.113	2.286
	inter-icosahedral	1	1.819	0.112	-0.176	0.313
	B2-B1	1	1.903	0.085	-0.052	2.271
B3	intra-icosahedral	5	1.814	0.111	-0.105	2.364
	inter-icosahedral	1	1.819	0.112	-0.176	0.313
B4	intra-icosahedral	5	1.778	0.117	-0.124	2.318
	B4-B1	1	1.674	0.156	-0.365	0.038
B5	intra-icosahedral	5	1.774	0.119	-0.128	2.369
	inter-icosahedral	1	1.661	0.158	-0.380	0.005

Table S2. Geometrical distances (Å) from (3,-1) bond critical points to their associated nuclear attractors in γ-B_{28}. Notice strong asymmetry of bond critical point location for the B1-B2 bond.

Atom	B1	B2	B3	B4	B5
B1	0.87; 0.87	**0.87; 1.04**		0.85; 0.83	
B2	**1.04; 0.87**	0.87; 0.87	0.93; 0.90 0.93; 0.92 0.94; 0.92	0.93; 0.88	0.93; 0.85
B3		0.90; 0.93 0.92; 0.93 0.92; 0.94	0.93; 0.93	0.90; 0.87	0.91; 0.88
B4	0.83; 0.85	0.88; 0.93	0.87; 0.90		0.89; 0.87
B5		0.85; 0.93	0.88; 0.91	0.87; 0.89	0.83; 0.83

Table S3. Geometrical distances (Å) from (3,-1) bond critical points to their associated nuclear attractors in γ-B_{28} using the IAM model. One can see that the bond critical point is always located close to the bond midpoint, even for the B1-B2 bond. Strong asymmetry appears only as a result of chemical bonding (Table S2).

Atom	B1	B2	B3	B4	B5
B1	0.87; 0.87	**0.94; 0.98**		0.83; 0.84	
B2	**0.98; 0.94**	0.87; 0.87	0.91; 0.91 0.92; 0.92 0.93; 0.93	0.91; 0.91	0.89; 0.89
B3		0.91; 0.91 0.92; 0.92 0.93; 0.93	0.93; 0.93	0.88; 0.89	0.89; 0.90
B4	0.84; 0.83	0.91; 0.91	0.89; 0.88		0.88; 0.88
B5		0.89; 0.89	0.90; 0.89	0.88; 0.88	0.83; 0.83

$5. Derivation of the LCAO basis sets.

Triple-ζ basis (Table S4). Starting from 6-21-(1*d*)G basis set (6-21G*), a 6-111-(1*d*)G basis set was obtained by splitting the two Gaussian type functions (GTFs) of the innermost valence *sp* shell and by using a scale factor of 1.2 for the exponent of the outermost valence GTF. A smaller scale factor (1.1) was also tested. Integrated charges are stable enough and the results reported here refer to the computation with a scale factor of 1.2. The exponent of the *d* function is 0.8 as in the original 6-21G* basis set.

Quadruple-ζ basis (Table S5). This 6-1111-(1*d*)G basis has the same 1*s* core description as the 6-21G basis, whereas the four *s*p valence shells are composed by a single GTF whose exponent is defined according to the rule of thumb of a factor of 3 between contiguous basis functions and starting from 0.17 as the lowest exponent. This latter was the lowest possible value to avoid linear dependency in both γ-B_{28} and α-B_{12}. The exponent of the *d* function is 0.8 as in the original 6-21G* basis set.

Quadruple-ζ basis from cc-pVQZ basis set (Table S6). The 1*s* and 1*s*' shells were left unchanged (so this basis has a double-ζ rather than a single-ζ description for the core). The outermost *s* and *p* functions of the cc-pVQZ have been removed because of linear dependency. The remaining four *s* and four *p* valence shells have been transformed in four *sp* shells, each composed of a single GTF whose exponent is defined according to the rule of thumb of a factor of 3 between contiguous basis functions and starting from 0.14 as the lowest exponent. This latter was the lowest possible value to avoid linear dependency in this case. A single d function (α=0.8), rather then four of them, was retained. No f and g functions.

$6. Basis set tables.

In the CRYSTAL-2006 code, each crystal orbital, $\psi_i(\mathbf{r};\mathbf{k})$ is a linear combination of Bloch functions, $\Phi_\mu(\mathbf{r};\mathbf{k})$, defined in terms of local functions, $\varphi_\mu(\mathbf{r})$, referred to as Atomic Orbitals (AOs). These local functions are then expressed as linear combinations of a certain number, *ng*, of individually normalised Gaussian type functions (GTFs), *G,* characterized by the same centre, fixed coefficients C_j ,and exponents, α_j, defined in the input:

$\varphi_\mu(\mathbf{r}) = \Sigma_{j=1,ng}\, C_j\, G(\alpha_j, k; \mathbf{r})$

$G(\alpha_j, k; \mathbf{r}) = N_{l,m}(\alpha_j)\, \chi_{l,m}(\mathbf{r}) \exp[-\alpha_j(k\mathbf{r})^2]$,

where $N_{l,mi}$ is a normalizing factor, depending also on the angular and magnetic quantum numbers, $\chi_{l,m}$ is a real solid spherical harmonic and k is the scaling factor. The AOs belonging to a given atom are grouped into *shells,* which contain all AOs with the same quantum number, *n* and *l* (for instance 2s, 2p, 3d shells) or all AOs with the same principal quantum number, *n*, if the number of GTFs and the corresponding exponents are the same for all of them (*sp* shells, also known as the s = p constraint). In the tables below, C_0, C_1, C_2 are the C expansion coefficients for *l*=0,1,2, respectively.

Table S4. Triple-ζ basis.

Shell (k)	α	C_0	C_1	C_2
s (1.0)	2082.0 312.3 70.89 19.85 6.292 2.129	0.00185 0.01413 0.06927 0.2324 0.4702 0.3603		
sp (1.0)	2.282	1.0	1.0	
sp (1.0)	0.4652	1.0	1.0	
sp (1.2)	0.1243	1.0	1.0	
d (1.0)	0.8			1.0

Table S5. Quadruple-ζ basis.

Shell (k)	α	C_0	C_1	C_2
s (1.0)	2082.0 312.3 70.89 19.85 6.292 2.129	0.00185 0.01413 0.06927 0.2324 0.4702 0.3603		
sp (1.0)	4.59	1.0	1.0	
sp (1.0)	1.53	1.0	1.0	
sp (1.0)	0.51	1.0	1.0	
sp (1.0)	0.17	1.0	1.0	
d (1.0)	0.8			1.0

Table S6. Quadruple-ζ basis from the cc-pVQZ basis set.

Shell (k)	α	C_0	C_1	C_2
s (1.0)	23870	0.000088		
	3575	0.000687		
	812.8	0.0036		
	229.7	0.014949		
	74.69	0.051435		
	26.81	0.143302		
	10.32	0.300935		
	4.178	0.403526		
	1.727	0.22534		
s (1.0)	23870	-0.000018		
	3575	-0.000139		
	812.8	-0.000725		
	229.7	-0.003063		
	74.69	-0.010581		
	26.81	-0.031365		
	10.32	-0.071012		
	4.178	-0.132103		
	1.727	-0.123072		
sp (1.0)	3.78	1.0	1.0	
sp (1.0)	1.26	1.0	1.0	
sp (1.0)	0.42	1.0	1.0	
sp (1.0)	0.14	1.0	1.0	
d (1.0)	0.8			1.0

$7. Additional experimental details.

Synthesis. As described in the paper, samples of γ-B_{28} were synthesized in BN capsules. In previous studies[28] BN has been proven to be non-reactive with crystalline boron up to at least 2000 K and, therefore, the BN capsules be suitable for synthesizing chemically pure boron phases at temperatures below 2000 K. The starting material for high pressure synthesis was 99.9999% chemically pure β-B_{106}. We have also tried to use metal (Pt) capsules for the high *P-T* synthesis. The product shows significant diffusion of Pt in the sample, colour change and heterogeneity. When BN capsule, which offers inert environment, was used, a very clean interface between the recovered sample and the capsule is observed under microscope, and the samples look very uniform in colour and texture. Conditions of synthesis were: 12 GPa and 1800 K (annealed during 30 minutes), 15 GPa and 1800 K (annealed during 60 minutes), and 20 GPa and 2000 K (annealed

during 10 minutes). The homogeneity of all γ-B_{28} samples was established by micro-Raman spectroscopy (Dilor XY system, 5 micron beam). The X-ray electron probe microanalysis (S400, Leica / PGT Spirit and SX-50 Camebax, Cameca) of the recovered samples has revealed that the impurities, if present in the γ-B_{28} samples, are at an undetectable level.

Diffraction pattern and Le Bail refinement. While full Rietveld refinement of the structure cannot presently be performed (small size of the samples, which are not perfect powders; low scattering of X-rays by boron), partial refinement validating our determination of lattice parameters was possible and its results are presented in Fig. S5. The cell parameters resulting from this refinement are a=5.056(1) Å, b=5.641(1) Å, c=6.995(1) Å and R_{wp}=2.46 %. The values from the standard indexing procedure are a=5.0544 Å, b=5.6199 Å, c=6.9873 Å. Theoretical values are a=5.043 b=5.612 Å, c=6.921 Å.

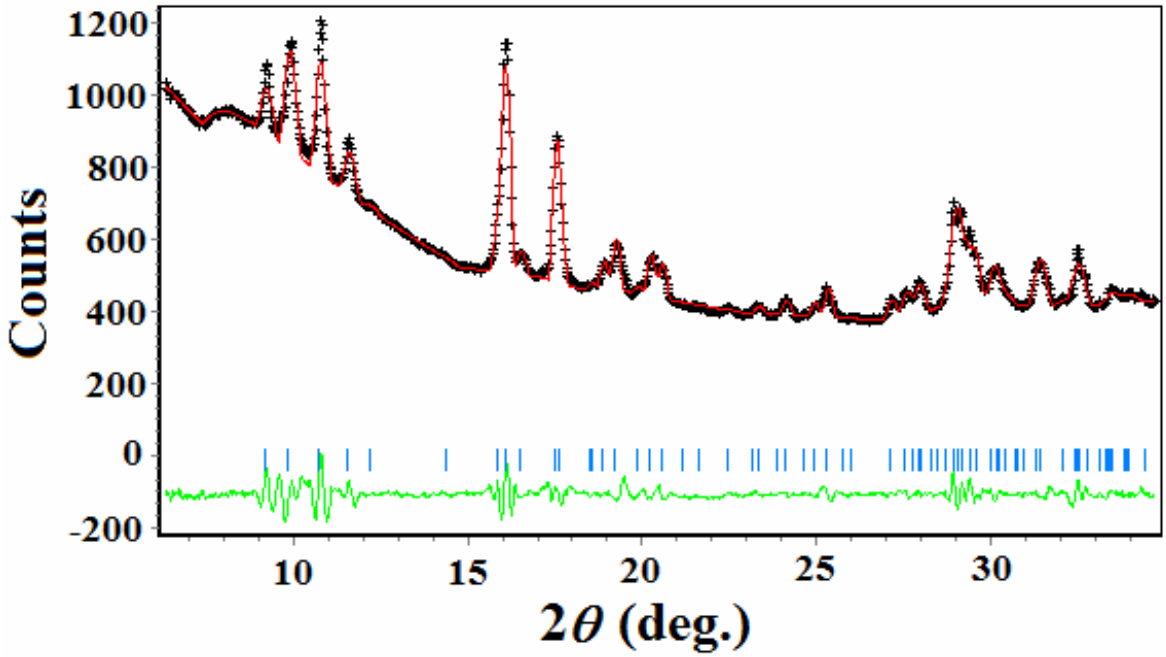

Fig. S5. Le Bail refinement of the powder diffraction spectrum of γ-B_{28}. The wavelength is λ=0.7307 Å. Red line and black crosses are calculated and observed data, respectively, and green line is their difference. Blue vertical bars show the expected peak positions.

References:

30. Oganov, A.R., Glass, C.W., Ono, S. High-pressure phases of $CaCO_3$: crystal structure prediction and experiment. *Earth Planet. Sci. Lett.* **241**, 95-103 (2006).

31. Perdew, J.P. & Wang, Y. Accurate and simple analytic representation of the electron-gas correlation energy. *Phys. Rev.* **B45**, 13244-13249 (1992).
32. Gatti, C., Saunders, V.R., Roetti, C. Crystal field effects on the topological properties of the electron density in molecular crystals: The case of urea. *J Chem Phys,* **101**, 10686-10696 (1994).
33. Gatti, C. TOPOND-98: An Electron Density Topological Program for Systems Periodic in N (N=0-3) Dimensions, User's Manual, CNR-ISTM, Milano (1999).
34. Sanville, E., Kenny, S.D., Smith, R., and Henkelman, G. An improved grid-based algorithm for Bader charge allocation, *J. Comp. Chem.* **28**, 899-908 (2007).